ACS OMEGA

http://pubs.acs.org/journal/acsodf

Article

Enhanced Biotribological and Anticorrosion Properties and Bioactivity of Ti6Al4V Alloys with Laser Texturing

Chenchen Wang,*,⊥ Panpan Tian,⊥ Hao Cao, Bin Sun, Jincan Yan, Yuan Xue, Hualin Lin, Tianhui Ren, Sheng Han,* and Xin Zhao*

Cite This: *ACS Omega* 2022, 7, 31081−31097

Read Online

ACCESS | Metrics & More | Article Recommendations | Supporting Information

ABSTRACT: The poor biotribological properties and bioinertness of Ti6Al4V have restricted its application in biomedical materials. In this study, microgrooves of different widths were prepared on the surface of a Ti6Al4V alloy by laser treatment. The tribological properties under dry lubrication and simulated body fluid (SBF) lubrication conditions, the electrochemical corrosion properties in SBF solution, and the bone marrow mesenchymal stem cell (BMSC) behavior on the surfaces were systematically tested. The corresponding mechanisms were discussed. The results showed that Ti6Al4V with a microgroove width of 45 μm (Ti64-45) exhibited excellent wear resistance with decreasing wear rates of 89.79 and 85.43% under dry friction and SBF lubrication compared to the Ti64 sample, which might be due to the increase of surface microhardness. Moreover, the excellent anticorrosion performance of Ti64-45 was attributed to the grain refinement on the titanium alloy surface with a lower volume fraction ratio of β phase to α phase. In addition, the microgrooves with a width of 45 μm are more conducive to BMSC proliferation and adhesion, related to promoting cell signal transduction due to cell extrusion. These studies imply that the microgroove structures are potential for application in the medical field.

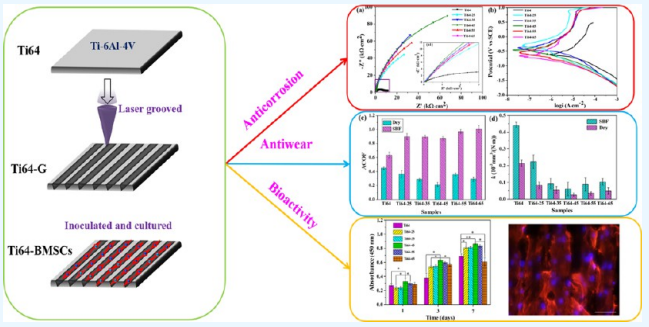

1. INTRODUCTION

Ti6Al4V is widely used for surgical implants. However, its poor wear resistance and biological inertia have a great effect on the service life of titanium alloy implants, especially bone implants.[1−4] The debris from wear and corrosion might react with bone tissues, leading to implant loosening.[5−7] Moreover, the weak interface bonding between the implant and bone also accelerates implant failure.[8,9] Therefore, it is necessary to improve the antiwear and anticorrosion properties and bioactivity of titanium alloys through surface modification.

Generally, surface treatment methods include surface texturing and surface coating techniques.[10−12] Among them, laser processing technology, as a popular surface texturing method, has been concerned due to its nontoxic, environmentally friendly, simple, feasible, accurate, and controllable features. Several research studies reported that the microstructures obtained by laser texturing technology have a positive effect on the surface properties of materials, such as the improvement of tribological behavior, electrochemical corrosion performance, and biological activity.[13−15] Wu et al.[16] studied the influence of laser texture micropatterns on the tribological properties of titanium alloys and pointed out that the antiwear properties of titanium alloys were significantly improved in the friction process. The reason might be attributed to the increasing bearing capacity and the function of capturing debris from the structure. Similar studies have been confirmed by other researchers.[17] Xu et al.[18] enhanced the corrosion resistance of the titanium alloy surface by laser processing. It was found that the effect of the treatment on the corrosion resistance of the surface was mainly due to the phase transformation of the substrate. Kumari et al.[19] also pointed out that the significant improvement of anticorrosion on the laser-treated material surface might be due to the surface grain refinement and homogenization of the microstructure. Furthermore, according to the previous research,[15] the laser-textured microstructure can affect the cell behavior and bone integration of implants. Some researchers have pointed out that among these microstructures, laser-microgrooved structures have a positive promotion effect on the tribological behavior, anticorrosion properties, and bioactivity of the material surface.[20−23] Therefore, texturing microgroove structures on the titanium alloy's surface is a feasible method for improving implant surface properties.

Received: May 21, 2022
Accepted: August 1, 2022
Published: August 24, 2022

https://doi.org/10.1021/acsomega.2c03166
ACS Omega 2022, 7, 31081−31097

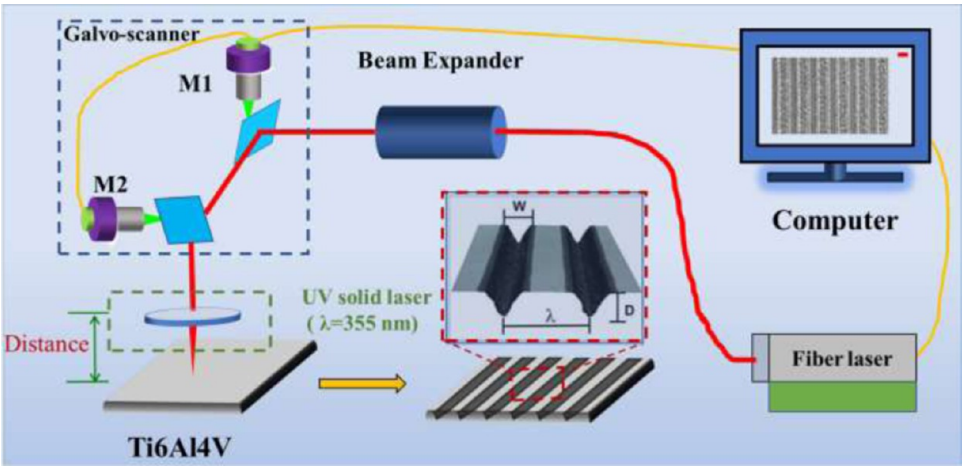

Figure 1. Schematic of the laser surface-microgrooved process on Ti6Al4V alloy plates.

Table 1. Surface-Microgrooved Laser Parameters

parameters	pulse speed (mm/s)	frequency (kHz)	power (W)	distance (cm)	scan times	spot diameter (μm)	laser energy density (J/cm^2)
Ti64-25	400	35	1.5	11.7	37	10	54.6
Ti64-35	300	30	2.5	12.4	42	5	424.4
Ti64-45	600	32	3	12.7	55	5	477.5
Ti64-55	300	30	2.7	12.0	50	10	114.6
Ti64-65	700	30	3	11.4	124	10	127.3

In addition, as previous reports described, the laser microgroove parameters might significantly affect the surface performance.[5,24] Several studies[25−28] indicated that the widths of microgrooves had an important effect on the wear resistance, corrosion resistance, and cell response of the material surface, and they pointed out that the difference in mechanical properties and the microstructure crystal phase structure are the main factors affecting surface properties. Bhaduri et al.[29] reported that the groove arrays with a width of 40 um effectively improved the tribological performance on tungsten carbide (WC) blocks. Moreover, Raimbault et al.[30] pointed out that cellular behavior was sensitive to the width of the microgroove, related to the arrangement and growth of cells. Gui et al.[31] prepared the grooves on the silicon substrate with a width of 5−20 μm and implied that the groove with a 20 μm width increased the number of osteoblast soars. However, there is no unified conclusion on the optimistic microgroove width, beneficial to the improvements of antiwear, anticorrosion, and bioactivity simultaneously. Therefore, it is necessary to investigate the effect of textured microgroove patterns on the enhancement of tribological properties, corrosion resistance, and biological activity.

In this study, microgrooves of different widths were processed on the surface of titanium alloy by adjusting UV nanosecond laser parameters. The morphology and chemical composition of the textured surface were characterized by scanning electron microscopy (SEM), laser confocal microscopy (LSCM), and X-ray diffraction (XRD). The effects of microgroove width on surface roughness, mechanical properties, and wettability of the titanium alloy were investigated. The biotribological properties in dry friction and SBF solution, corrosion resistance, and bone marrow mesenchymal stem cell (BMSC) behavior of the titanium alloy with different groove widths were evaluated. The corresponding mechanisms of antiwear, anticorrosion, and bioactivity were analyzed through surface characterization.

2. MATERIALS AND METHODS

2.1. Materials. Ti6Al4V alloy plates (medical grade, referred to as Ti64) were purchased from Baoji Junhang Metal Material Co., Ltd. and the chemical composition of the Ti6Al4V alloy is listed in Table S1. They were machined into dimensions of 10 mm × 10 mm × 2 mm (length × width × thickness) by wire cutting, and polished to a roughness (R_a) of 0.2 ± 0.02 μm. They were ultrasonically cleaned with deionized water and anhydrous ethanol three times, respectively. Si_3N_4 ceramic ball was purchased from Shanghai Wha Bearing Co., Ltd. Acetone, anhydrous ethanol, and other solvents in this work are analytically pure, purchased from Shanghai Sinopharm Group Co., Ltd. Simulated body fluid (SBF) was purchased from Xian Hutt Biological Co., Ltd. Its solution composition is shown in Table S2. Fetal bovine serum was purchased from Gibco. Paraformaldehyde, penicillin, streptomycin, 4′,6-diguinyl-2-phenyl indole, and rhodamine ghost pen ring peptide were purchased from Sigma-Aldrich. Cell counting kit-8 was purchased from Dojindo Laboratories in Kumamoto, Japan.

2.2. Laser Equipment and Parameters. A UV nanosecond laser (Shanghai Fermi Laser Processing Co., Ltd.) with a wavelength of 355 nm and total power of 5 W was applied to process a microgroove structure on the surface of a Ti6Al4V alloy plate. The schematic diagram of the principle is shown in Figure 1. Microgroove patterns with different widths were obtained by adjusting the laser processing parameters. The corresponding laser parameters are shown in Table 1. The laser-processed titanium alloy samples were referred to as Ti64-25, Ti64-35, Ti64-45, Ti64-55, and Ti64-65, according to the width of the microgrooves. The textured parameters of the sample can be marked as width (W), spacing (λ), and depth (D). At the same time, the corresponding laser energy densities (E) were calculated by formula 1, respectively.[32] The prepared samples were ultrasonically cleaned with acetone and deionized water for 15 min.

https://doi.org/10.1021/acsomega.2c03166
ACS Omega 2022, 7, 31081−31097

$$E = \frac{P}{Z\pi r^2} \quad (1)$$

where E is the laser energy density, P is the average power, Z is the frequency, and r is the spot radius.

2.3. Surface Wettability Measurement. The static contact angle (CA) of the sample surface was measured by the droplet suspension method with a contact angle tester (DSA30, Kruss, German). The wettability of the titanium alloy surface was further evaluated by calculating the CA value. The detail test method was as follows: the deionized water was dropped on the surface of Ti64, Ti64-25, Ti64-35, Ti64-45, Ti64-55, and Ti64-65 sample plates. The CA value of the sample surface is obtained by calculating the spherical approximate value of the surface droplet. Each group of samples was tested five times and the average value was taken.

2.4. Surface Microhardness Measurement. A Vickers hardness tester (MC010-HVS-1000, China) was used to measure the surface hardness of Ti64, Ti64-25, Ti64-35, Ti64-45, Ti64-55, and Ti64-65 sample plates. The set load was 100 g. Samples were tested five times under each condition and the obtained average value was the final microhardness.

2.5. Electrochemical Corrosion and Biotribological Property Tests. To study the influence of the microgroove structure on the corrosion resistance of the titanium alloy surface in SBF solution, the electrochemical corrosion behavior of sample plates (Ti64, Ti64-25, Ti64-35, Ti64-45, Ti64-55, Ti64-65) in SBF solution at 37 °C was tested by an electrochemical workstation (CHIT60E, Shanghai Chenhua Co., Ltd.). Moreover, the corrosion potential and self-corrosion current density of the samples were analyzed through the workstation.

The tribological tests of titanium alloy samples were recorded using a tribometer (UMT-3, Bruker). The test module was a reciprocating ball−plate module. The test conditions of the sample under dry friction and SBF solution lubrication were as follows: room temperature, applied load 1 N, frequency 1 Hz, amplitude 2 mm, and test time 1800 s. As shown in the schematic diagram of tribological measurements (Figure 2),[8,9]

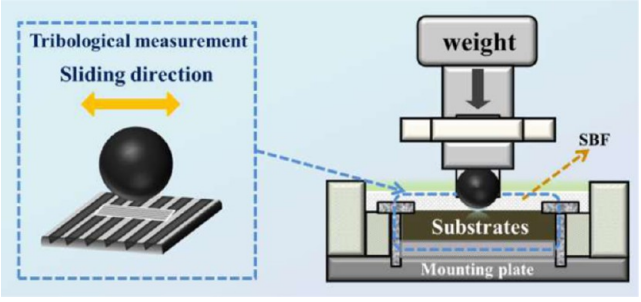

Figure 2. Schematic diagram of biotribological measurements using a tribometer.

the upper friction pair was a Si_3N_4 ball (Φ 6 mm), with a R_a of 0.02 μm and a Vickers hardness of 1500 HV. The titanium alloy sample was the lower friction pair. The real-time friction coefficient curve was automatically recorded by a computer. Each group of tribological tests was tested three times, and the average value of the average friction coefficient was taken as the final data.

After the friction tests were completed, the wear rate (k, mm^3/(N·m)) of the surface of those titanium alloy samples was calculated according to formula 2.[8]

$$k = \frac{V}{X \cdot F_N} \quad (2)$$

where V is the wear volume, X is the sliding distance, and F_N is the applied load.

2.6. In Vitro Bioactivity Test. The cell evaluation experiment on the titanium alloy surface before and after the microgroove treatment follows the principles of the Declaration of Helsinki. Before the experiment, six groups of titanium alloy plates (including Ti64, Ti64-25, Ti64-35, Ti64-45, Ti64-55, and Ti64-65) were sterilized at high temperatures and high pressures. In addition, the BMSCs were isolated from female C57BL/6 mice aged 4−6 weeks. First, BMSCs were washed out of the tibia and femur of the mouse by MEM Alpha modification (α-MEM) in a sterile environment. Subsequently, the cells were centrifuged at 1000 rpm for 8 min, and cultured in α-MEM containing 10% fetal bovine serum and 1% penicillin and streptomycin, and the temperature was controlled to 37 °C. After the cells were cultured for 3 days, the original medium was replaced with a fresh medium. The cell confluence rate reaches 80−90% for the following cell proliferation experiments.

To evaluate the cell viability of BMSCs on the titanium alloy sample plates, BMSCs (2×10^4 cells/mL) were inoculated on 24-well culture plates containing different samples. After 1, 3, and 7 days of culture, according to the manufacturer's instructions, the activity of BMSCs on the samples was quantitatively tested with a cell counting kit-8 (CCK-8). In addition, the adhesion performance of BMSCs on Ti64, Ti64-25, Ti64-35, Ti64-45, Ti64-55, and Ti64-65 samples was studied. First, BMSCs were inoculated and cultured on the sample plates. After 1 day, the cells on the sample plates were fixed with 4% paraformaldehyde for 15 min. Subsequently, the fixed cells were washed three times with a phosphate buffer solution. After that, the cells were cultured in DAPI solution for 5 min to stain the nuclei. The cytoskeleton was stained by immersing in rhodamine cyclopeptide solution for 30 min. Finally, the cells that adhered to the sample surface were characterized with a fluorescence microscope. In the fluorescence image, the nucleus is marked in blue color and the cytoskeleton is marked in red color.

2.7. Analysis Methods. The microstructure and chemical composition on the surfaces of these titanium alloy samples before and after texturing were characterized by a scanning electron microscope (SEM, FEI Nova 450) and an energy-dispersive X-ray spectrometer (EDX) at 10 kV voltage. The three-dimensional topography of the sample surface was characterized by a confocal laser microscope (CLM, VK-X100). VK analysis software was used to measure the surface roughness of titanium alloys with different microgroove widths.

X-ray diffractometer (XRD, D8 Advance, Germany) was used to analyze the crystal phase state of Ti64, Ti64-25, Ti64-35, Ti64-45, Ti64-55, and Ti64-65 samples. To obtain the ratio of the volume fraction of the α phase to the β phase on the sample surface, Origin 9.1 software was applied to fit the XRD spectra of each sample.[33] According to formulas 3 and 4, the volume fraction of the α phase and the volume fraction ratio of the α phase to the β phase can be calculated, respectively.[18]

$$\varphi_\alpha = \frac{S_\alpha}{S_\alpha + S_\beta} \quad (3)$$

$$\varphi = \frac{\varphi_\beta}{\varphi_\alpha} \quad (4)$$

https://doi.org/10.1021/acsomega.2c03166
ACS Omega 2022, 7, 31081−31097

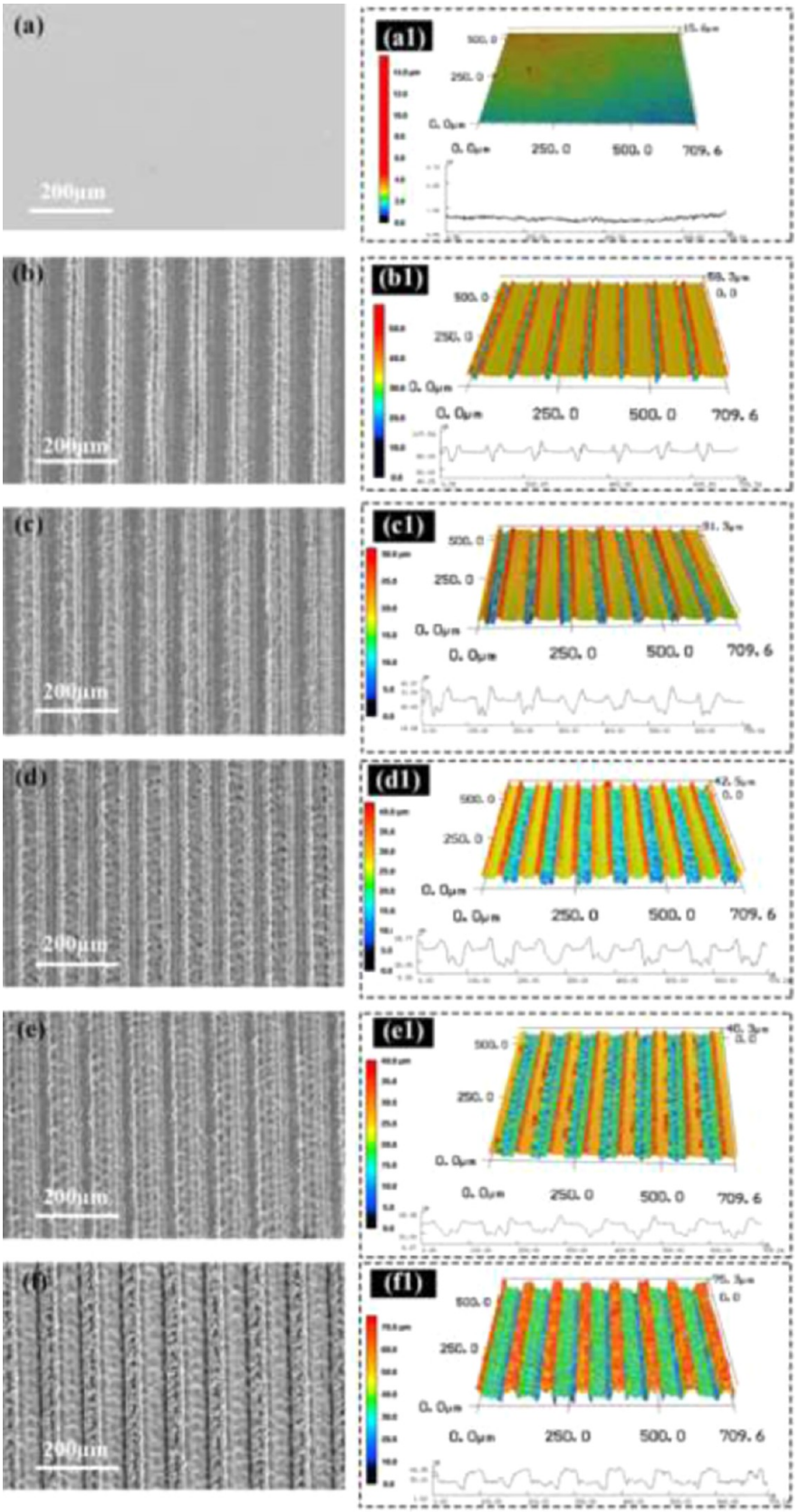

Figure 3. Surface morphologies of titanium alloy specimens before and after texturing. (a−f) SEM images of Ti64, Ti64-25, Ti64-35, Ti64-45, Ti64-55, and Ti64-65 plates; (a1−f1) 3D topography of Ti64, Ti64-25, Ti64-35, Ti64-45, Ti64-55, and Ti64-65 plates.

where φ_α is the volume fraction of the α phase on the titanium alloy, S_α and S_β are, respectively, the sum of the peak areas of the α phase and the β phase (the 2θ angle range is 34−43°), and φ is the volume ratio of the β phase to the α phase.

https://doi.org/10.1021/acsomega.2c03166
ACS Omega 2022, 7, 31081−31097

A three-dimensional optical profiler (white light interferometer, WLI, Contour GT-K0, Bruker, Germany) was conducted to test the 3D profile and wear rate of the worn surface of the samples.

3. EXPERIMENTAL RESULTS

3.1. Morphological Characterization. The surface morphology of the titanium alloy treated with UV nanosecond laser treatment was characterized by SEM and CLM, as shown in Figure 3. It can be seen from Figure 3a−f (SEM images) that the groove patterns with different groove widths were obtained on the surface of the titanium alloy by controlling the laser texturing parameters. Moreover, a small amount of deposition was observed on the edge of the microgrooves of the titanium alloy. This might be attributed to the formation of a remelting layer on the titanium alloy surface after the thermal effect during laser processing. Figure 3a1−f1 shows the three-dimensional topography of Ti64, Ti64-25, Ti64-35, Ti64-45, Ti64-55, and Ti64-65 samples. The corresponding sample parameters were measured and are listed in Table 2. It can be seen from Table 2 that the groove width (W) and the groove spacing (λ) are precisely controlled during the laser treatment. The depth (D) was in the range of 9−13 μm.

Table 2. Parameters of Microgrooved Ti6Al4V Alloy Plates[a]

samples	W (μm)	λ (μm)	D (μm)
Ti64-25	25	100	10.4
Ti64-35	35	100	9.8
Ti64-45	45	100	11.1
Ti64-55	55	100	10.9
Ti64-65	65	100	12.3

[a]Note: W represents the width of the textured microgroove, λ represents the spacing of the textured microgroove, and D represents the depth of the textured microgroove, with a range of 9−13 μm.

3.2. Surface Roughness of Titanium Alloy Samples. The surface roughness of titanium alloy samples before and after laser processing were analyzed and are listed in Table 3. This mainly includes the arithmetic mean deviation of the contour (R_a), the root-mean-square value of the deviation of the contour mean line (R_q), and the maximum height of the contour (R_z). Among them, R_a and R_q are the most important evaluation parameters. It can be seen from Table 3 that the R_a and R_q of the titanium alloy samples showed the same sequence as follows: Ti64 < Ti64-25 < Ti64-35 < Ti64-55 < Ti64-45 < Ti64-65. According to previous reports, the changes in the surface roughness of laser-textured samples were mainly attributed to two important laser parameters: laser intensity and pulse overlap times.[34,35] According to the laser parameters listed in Table 1, it can be found that with the increasing groove width, the required laser power and the number of pulse overlaps exhibited an increasing trend. However, the fact that the surface roughness of Ti64-45 was slightly larger than that of the Ti64-55 sample, might result from the higher laser power (laser power of 3 W) and more pulse overlaps (55 times) on Ti64-45 than that on Ti64-55 (laser power of 2.7 W) and the number of pulse overlaps (50 times).

Table 3. Surface Roughness of Titanium Samples

samples	R_a (μm)	R_q (μm)	R_z (μm)
Ti64	0.19	0.23	1.17
Ti64-25	3.09	4.99	58.29
Ti64-35	3.39	4.66	31.29
Ti64-45	6.43	7.80	42.52
Ti64-55	6.37	7.38	39.96
Ti64-65	10.73	13.43	80.45

3.3. XRD Characterization of Titanium Alloy Samples. To analyze the effect of ultraviolet laser treatment on the crystalline state of the titanium alloy surface, Figure 4 shows the partial XRD spectrum of titanium alloy specimens before and after texturing. The corresponding crystal plane diffraction peaks are marked and two phases (α phase (hcp) and β phase (bcc)) are observed in this figure. It can be clearly seen from Figure 4 that after laser processing, the intensity of the 002 hcp peak on the surface of the titanium alloy sample reduced, while the intensity of the 101 hcp peak increased. Moreover, compared with the Ti64 sample, a wider diffraction peak was observed on the surface of the microgrooved titanium alloy, which is consistent with previous reports.[18] In addition, the volume fraction ratio of the α phase and β phase was calculated by fitting the peak areas of the α and β phases (α phase is the yellow area and β phase is the red area). The results are shown in Table 4. The volume ratio (φ) of the β phase to the α phase (φ%) was sorted as follows: Ti64-45 (5.51%) < Ti64-35 (11.16%) < Ti64-65 (11.54%) <Ti64-55 (13.11%) < Ti64-25 (14.25%) < Ti64 (14.74%). It was found that laser treatment significantly reduced the volume fraction ratio of the β phase to the α phase on the titanium alloy surface, further implying that the titanium alloy surface was transformed from the β phase to the α phase after laser ablation. Among them, the phase transformation on the surface of the Ti64-45 sample was more obvious with a lower volume ratio (φ: 5.51%).

The results might be further explained by the Burgers orientation relationship.[33,36] The surface temperature of the Ti6Al4V alloy would increase rapidly to above 882.5 °C during the laser ablation process, resulting in the remelting of the heat-affected zone on the surface of titanium alloys. After that, as the surface temperature of the titanium alloy reduced rapidly, the body-centered cubic structure (β phase) of the surface crystals would partially transfer to the hexagonal lattice structure (α phase). Moreover, the previous reports[37,38] indicated that the phase transformation on these samples was related to the laser energy density during the laser processing. Compared with the laser-treated titanium alloy samples, it can be found from Tables 1 and 4 that the laser-microgrooved samples treated with a larger E value exhibited a lower β/α value, and Ti-45 showed the highest E value. Zafari et al.[37] pointed out that a larger laser energy density would lead to a large thermal gradient and a faster cooling rate. It is known that due to the rapid solidification, the microstructure of the laser-textured part is prone to form very fine needles of α' prime martensite rather than forming the β phase during the remelting process.[26] Therefore, Ti-45 has the lowest β/α content. Besides, with the increase of laser energy density, the lamella width of a single α phase decreased, while the smaller columnar crystal width increased.[38] Therefore, after laser treatment, the grain microstructures were refined, and Ti-45 with a higher E value might exhibit a more refined microstructure.

3.4. Surface Wettability of Titanium Alloy Samples. As shown in Figure 5, the effect of laser treatment on the wettability of the titanium alloy surface was evaluated by calculating the contact angle of water droplets on the surface of the sample. The wetting behavior of the sample surface might be affected, due to

https://doi.org/10.1021/acsomega.2c03166
ACS Omega 2022, 7, 31081−31097

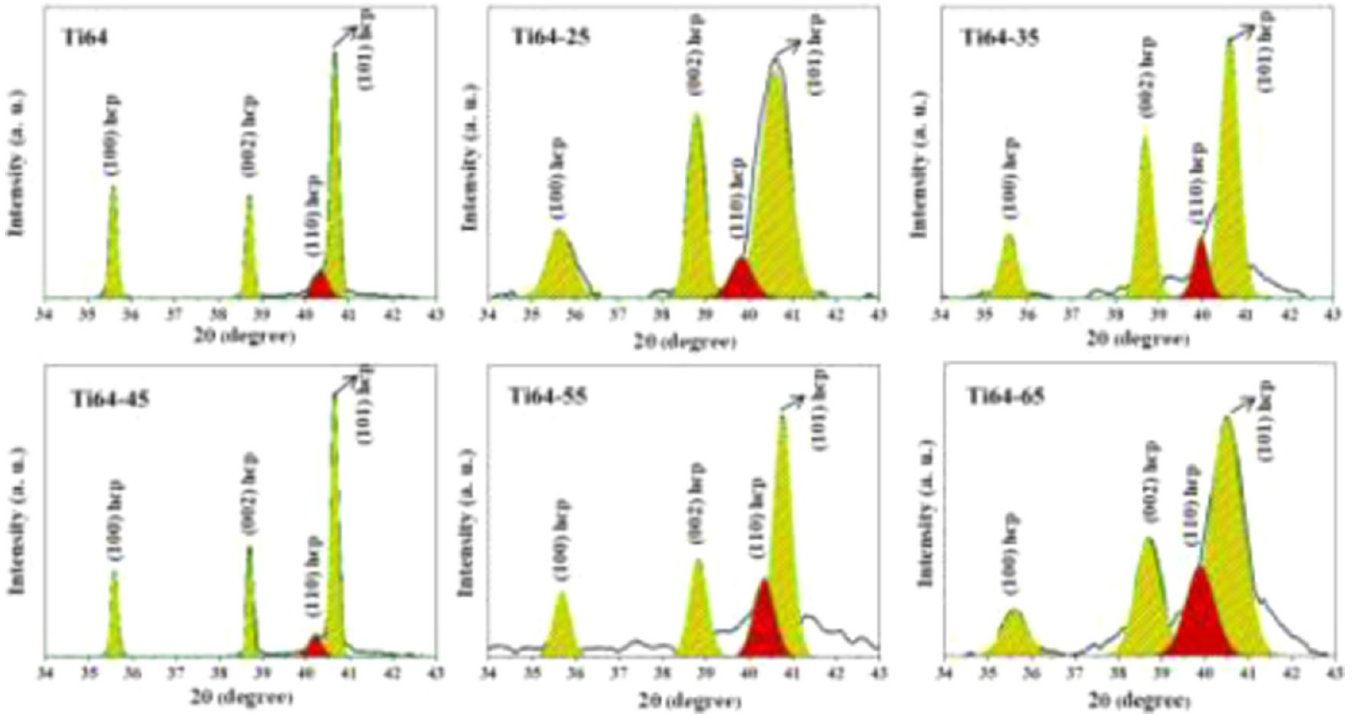

Figure 4. XRD spectrum magnifications of titanium alloy specimens before and after texturing, including Ti64, Ti64-25, Ti64-35, Ti64-45, Ti64-55, and Ti64-65 plates.

Table 4. Phase Volume Fraction of Titanium Alloy Samples

samples	phase	φ_α (%)	φ_β (%)	φ (%)
Ti64	$\alpha + \beta$	87.15	12.85	14.74
Ti64-25	$\alpha + \beta$	88.41	12.47	14.25
Ti64-35	$\alpha + \beta$	89.65	10.04	11.16
Ti64-45	$\alpha + \beta$	94.78	5.22	5.51
Ti64-55	$\alpha + \beta$	87.53	11.59	13.11
Ti64-65	$\alpha + \beta$	89.96	10.35	11.54

the anisotropy of the surface microgroove pattern.[39] According to the observation directions, the contact angles were abbreviated as contact angle perpendicular to the groove direction (VCA) and the contact angle parallel to the groove direction (PCA). It can be seen from Figure 5a that the VCA value of the titanium alloy surface decreased after laser treatment. Moreover, as the groove width increased, the VCA value exhibited a decreasing trend, suggesting the improving surface wettability. This might be ascribed to the fact that the groove structure with a certain depth has the function of storing water droplets, making it easier to spread the water droplets on the surface of the titanium alloy and exhibiting a lower contact angle. Moreover, as the width of the microgrooves increased, the volume of the stored water droplets increased and the contact angle decreased. The contact angle parallel to the groove direction is shown in Figure 5b. It can be intuitively found that the PCA values of Ti64-25 and Ti64-35 were higher than those of the untreated titanium alloy samples. The reason was ascribed to the anisotropic wettability of the laser microgroove structure, which is consistent with the previous report.[39] The squeezing effect on the water droplets of the groove structure would lead to a larger PCA value. Therefore, the above results indicated that the surface wettability of Ti6Al4V was enhanced through texturing the groove structure with a width greater than 45 μm.

3.5. Microhardness of Titanium Alloy Samples. Figure 6 shows the microhardnesss of titanium alloy samples before and after laser treatment. It can be seen that compared with the Ti64 sample, the microhardness of the grooved titanium alloy surface

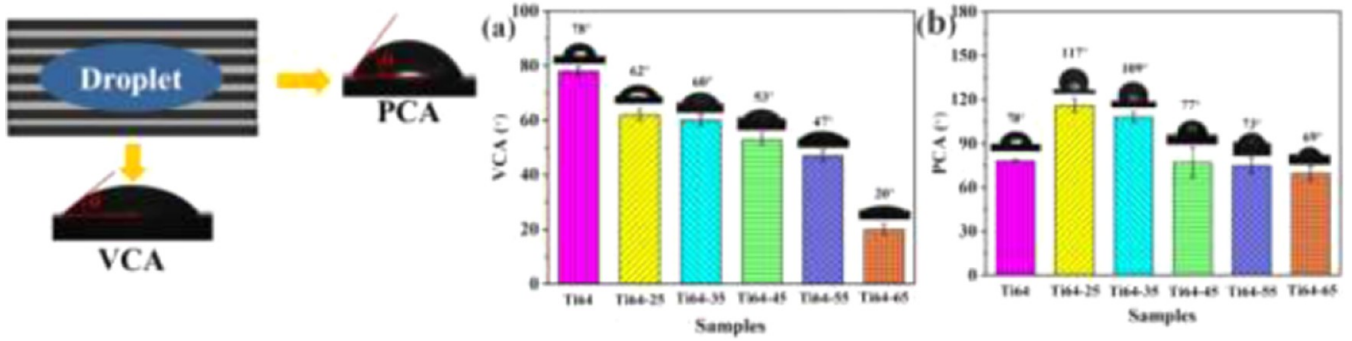

Figure 5. Measurement of wetting properties on the titanium alloy specimens before and after texturing. (a) CA values in the vertical observation, referred to as VCA and (b) CA values in the parallel observation, referred to as PCA.

https://doi.org/10.1021/acsomega.2c03166
ACS Omega 2022, 7, 31081−31097

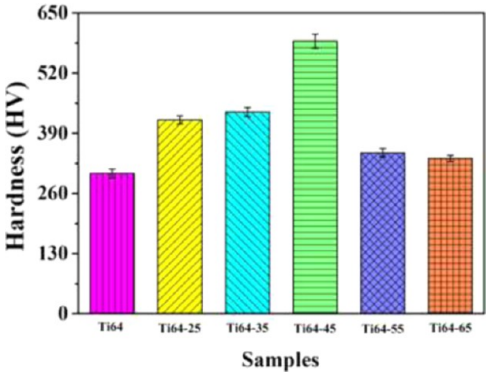

Figure 6. Measurement of microhardness on the titanium alloy specimens before and after texturing.

was significantly increased, in the following sequence: Ti64-45 (599 HV) > Ti64-35 (437 HV) > Ti64-25 (416 HV) > Ti64-55 (349 HV) > Ti64-65 (336 HV) > Ti64 (303 HV). It can be calculated that the microhardness of Ti64-45 increased by 97.7%, exhibiting the highest microhardness. This might be related to the organization's homogenization on the surface after laser texturing. As described in the XRD spectrum analysis (Figure 4), it was found that the obvious transfer of the crystal phase from the β phase to the α phase appeared on the Ti64-45 sample. This phase transformation would further refine the grain of the titanium alloy and hinder the movement of dislocations, thus increasing the surface microhardness.

3.6. Corrosion Resistance Performance. To evaluate the effect of laser-grooved treatment on the corrosion resistance of the titanium alloy surface, the electrochemical corrosion performance of the samples in the SBF solution was tested. The results are shown in Figure 7 and Table 5. Figure 7 shows the Nyquist impedance diagram and Tafel curve of the Ti6Al4V samples before and after the surface microgrooves. According to the previous report,[8] the larger the radius of curvature in the Nyquist impedance diagram, the better the corrosion resistance of the sample surface. It can be seen from Figure 7a1 that the radius of curvature of the microgrooved titanium alloy sample was significantly larger than that of the blank titanium alloy plate, in the following order: Ti64-45 > Ti64-35 > Ti64-65 > Ti64-55 > Ti64-25 > Ti64. This implied that laser texturing treatment improved the corrosion resistance of the titanium alloy surface.

Table 5. Electrochemical Corrosion Parameters of Titanium Alloy Plates in SBF Solution

samples	corrosion potential (mV)	corrosion current density (A/cm^2)	inhibition efficiency (%)
Ti64	−576	1.902×10^{-6}	
Ti64-25	−421	1.710×10^{-6}	10.09
Ti64-35	−475	9.525×10^{-7}	49.92
Ti64-45	−495	7.189×10^{-7}	62.20
Ti64-55	−527	1.440×10^{-6}	24.29
Ti64-65	−612	1.169×10^{-6}	38.54

Figure 7b is the Tafel curve of these samples. The fitting corrosion current density (i_{corr}), corrosion potential, and inhibition efficiency (refer to formula 5[28]) were calculated and shown in Table 5. It was found that the corrosion current of the samples has a negative correlation with the radius of curvature. Among them, the corrosion current density of the Ti64-45 sample was the smallest (7.189×10^{-7}) compared with the Ti64 sample (1.902×10^{-6}). Moreover, Ti64-45 exhibited a higher inhibition efficiency (62.20%), further suggesting the excellent corrosion resistance of Ti64-45 samples.

$$\eta\% = \frac{i_{corr}(\text{untreated}) - i_{corr}(\text{grooved})}{i_{corr}(\text{untreated})} \quad (5)$$

where i_{corr} (untreated) and i_{corr} (grooved) are the corrosion current density values without and with the coating, respectively.

3.7. Biotribological Properties. Figure 8 shows the tribological properties of the titanium alloy before and after the surface texturing in dry friction and SBF lubrication conditions. Among them, the variation curves of friction coefficients (COF) with the time of the six group samples during the dry friction and SBF lubrication process are, respectively, displayed in Figure 8a,b. It can be seen from these figures that after a running-in period during the friction process, the COF curve trend stabilizes with the extension of time under both lubrication environments. The corresponding average friction coefficient (referred to as ACOF) is shown in Figure 8c and Table 6. It can be found that under dry friction conditions, the friction coefficient of the microgrooved titanium alloy surface was lower than that of the untreated titanium alloy sample. Moreover, the groove width has a significant effect on the reduction of COF. Among these microgrooved samples, the

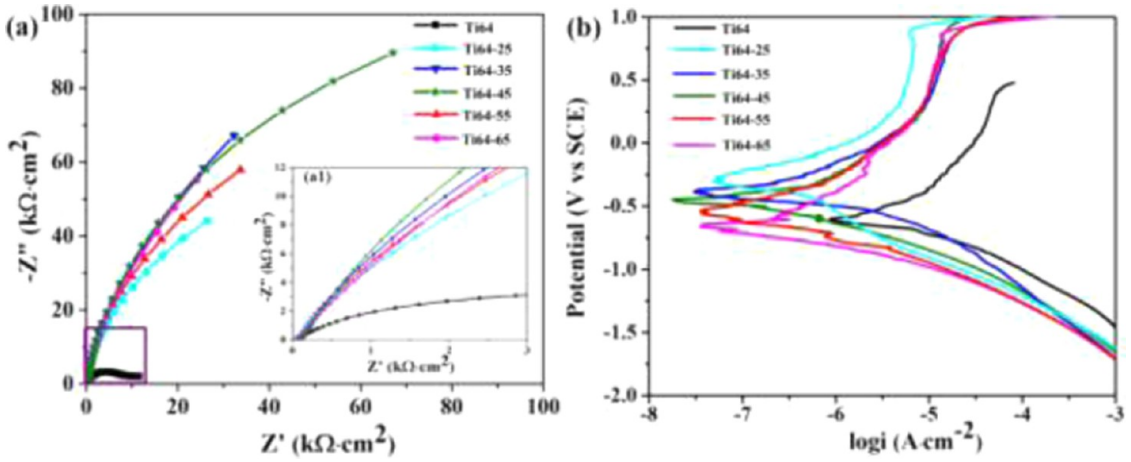

Figure 7. Anticorrosion property measurements on the titanium alloy specimens before and after texturing. (a) Nyquist plots, including the magnification (a1) of the six different plates and (b) Tafel plots of the six different plates.

https://doi.org/10.1021/acsomega.2c03166
ACS Omega 2022, 7, 31081−31097

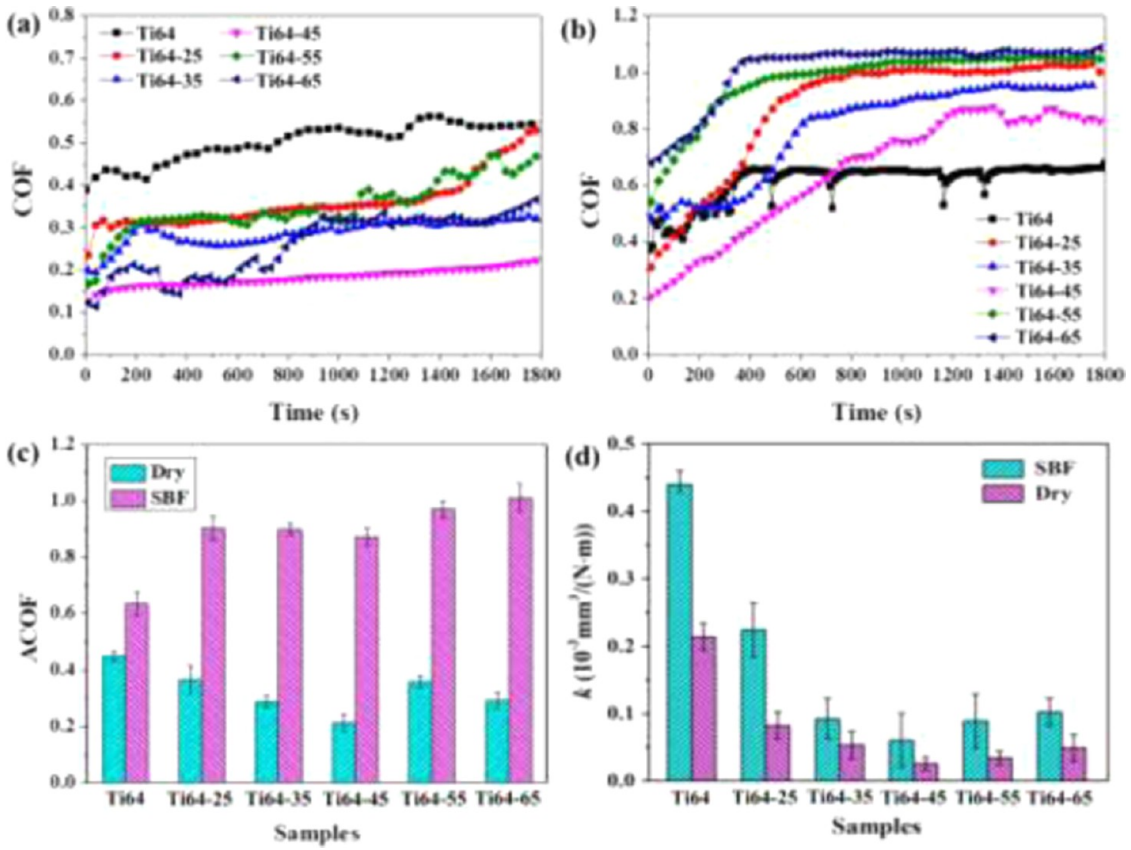

Figure 8. Coefficient of friction (COF) and wear rates of titanium alloy specimens before and after texturing under dry friction and SBF lubrication conditions. (a) Change of COF with sliding time under dry conditions; (b) change of COF with sliding time in SBF lubrication; (c) average coefficient of friction (ACOF) under both conditions; and (d) wear rates of the five plates.

Table 6. Frictional Performance Parameters of Samples under Dry Friction Conditions

samples	average coefficient of friction	wear rate, 10^{-3} mm^3/(N·m)	ratio of the reducing wear rate (%)
Ti64	0.435	0.235	
Ti64-25	0.469	0.078	66.80
Ti64-35	0.289	0.053	77.45
Ti64-45	0.215	0.024	89.79
Ti64-55	0.359	0.034	85.53
Ti64-65	0.290	0.047	80.00

Table 7. Frictional Performance Parameters of Samples under SBF Lubrication Conditions

samples	average coefficient of friction	wear rate, 10^{-3} mm^3/(N·m)	ratio of the reducing wear rate (%)
Ti64	0.526	0.446	
Ti64-25	0.901	0.252	43.50
Ti64-35	0.897	0.083	81.39
Ti64-45	0.872	0.065	85.43
Ti64-55	0.969	0.081	81.84
Ti64-65	1.011	0.101	77.35

Ti64-45 sample showed the lowest ACOF value (0.215), implying excellent antifriction properties in dry conditions. While under SBF lubrication, the friction coefficient of the titanium alloy has not been effectively reduced after laser-grooved treatment. The above results indicated that the microgroove structure, especially with the groove width of 45 μm, can effectively reduce the friction coefficient on the Ti6Al4V substrate in dry sliding friction.

The surface wear rates on these titanium alloys during the friction process were calculated and displayed in Figure 8d and Table 7. It can be found that the wear rates of the six groups of titanium alloy samples in SBF lubricants were higher than those in the dry friction process. Moreover, a similar change trend in the wear rate on the titanium alloy sample was observed (see Figure 8a). The wear rates presented a trend of first increasing and then decreasing with the increase of groove width. Compared with other samples, the Ti64-45 sample showed the lowest wear rate (0.042×10^{-3} mm^3/(N·m) in dry sliding and 0.065×10^{-3} mm^3/(N·m) in SBF sliding), with the reduction of 89.79% under dry friction and 85.43% in SBF lubrication compared to the Ti64 sample. Therefore, it can be concluded that a microgroove structure with a suitable groove width (45 μm) can effectively reduce the COF in dry sliding and improve the wear resistance of the titanium alloy substrate.

3.8. Surface Analysis of Wear Scars. The surface morphology of the wear scars was characterized by SEM and white light interferometry, and the chemical composition of the surface was analyzed by EDX. The characterization results are shown in Figures 9−11.

The three-dimensional morphologies of the surface wear scar on the titanium alloy sample under dry friction and SBF lubrication friction are exhibited in Figure 9. It can be seen from Figure 9a−f that serious wear with a maximum wear scar depth of ~5.5 μm appeared on the surface of the titanium alloy plate, after the sliding friction in a dry environment. After laser processing, with the increase of groove width, the wear depth

https://doi.org/10.1021/acsomega.2c03166
ACS Omega 2022, 7, 31081−31097

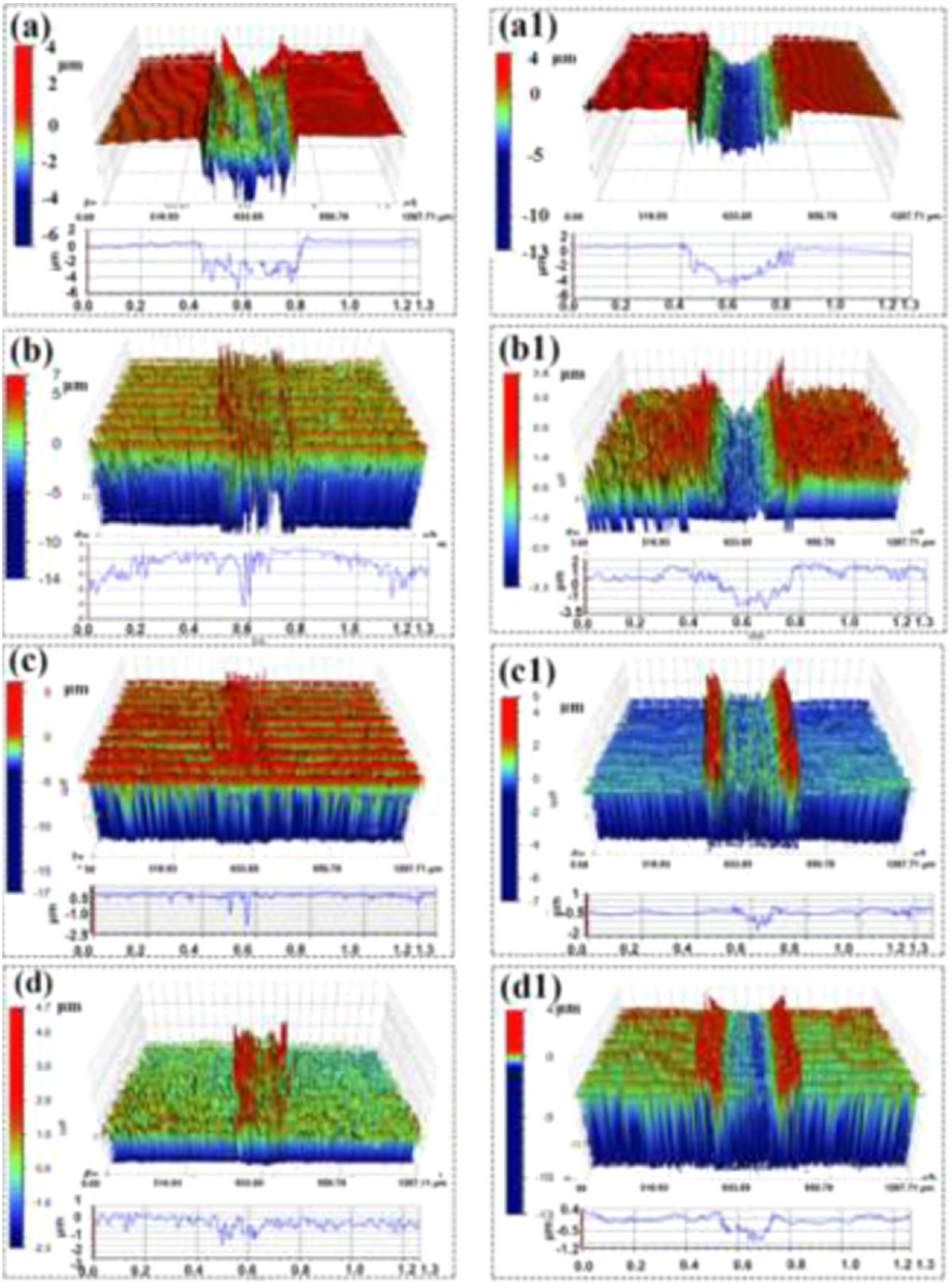

Figure 9. continued

https://doi.org/10.1021/acsomega.2c03166
ACS Omega 2022, 7, 31081−31097

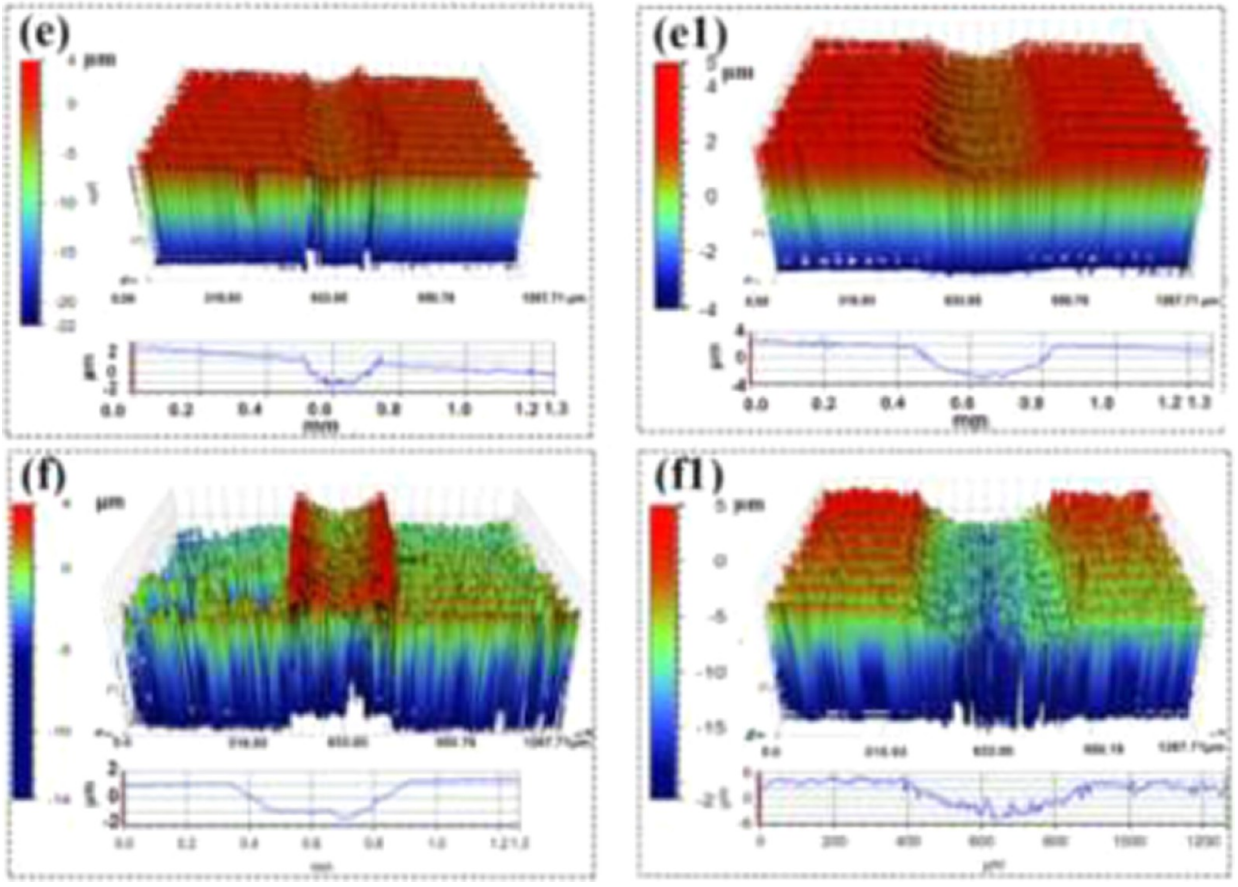

Figure 9. 3D topography of worn scars on the Ti−6Al−4V plates before and after texturing under dry friction conditions (a−f) and under SBF lubrication conditions (a1−f1). (a, a1) Ti64; (b, b1) Ti64-25; (c, c1) Ti64-35; (d, d1) Ti64-45; (e, e1) Ti64-55; and (f, f1) Ti64-65.

decreased preferentially and then increased. Ti64-45 had a smaller wear scar with a slighter wear depth of ∼1.5 μm. Under SBF lubrication conditions, the wear depth of the titanium alloy samples has a similar trend to that in dry friction, as shown in Figure 9a1−f1. It can be clearly seen from the figure that the wear trace of the blank titanium alloy plate (∼6 μm) is deeper than that of other samples. The grooved samples have relatively shallow wear marks, specially Ti64-45 with a wear depth of ∼2.5 μm. In addition, it can be observed that the depth of wear scars of each sample under SBF friction conditions was greater than that under dry sliding friction conditions. These characterization results were consistent with the change trend of the wear rates (Figure 8d).

Figure 10 shows the microscopic morphology and the corresponding chemical composition analysis results on the six groups of titanium alloy samples in dry friction. It can be seen from the SEM images (Figure 10a−f) that the blank titanium alloy plate has the widest wear scar width (∼398 μm) with serious material loss and obvious scratches, debris, and plows on the surface. This indicated that the abrasive wear occurred on the titanium alloy samples during the dry friction process. After the surface of the titanium alloy was grooved by laser treatment, the wear scar width was narrowed with reduced wear damage. Furthermore, as the groove width increased, the wear scar width showed a trend of first decreasing and then increasing. This corresponded to the change trend of the sample wear rate under dry friction (Figure 8d). In addition, the corresponding component analysis results of the surface of the titanium alloy samples are shown in Figure 10a2−f2. Si and N were detected on the wear surfaces of the six sets of titanium alloy samples, indicating the existence of Si_3N_4 transfer during the dry friction process and further implying the adhesive wear mechanism. Moreover, the contents of Si and N on the wear surface of the grooved titanium alloy were less than those on the Ti64 sample, demonstrating that the surface groove treatment might effectively reduce the adhesive wear. Among them, the Si content of the worn surface of the Ti64-45 sample exhibited the lowest value (0.82 wt %), suggesting a slight adhesive wear behavior.

Figure 11 exhibits the SEM images and the corresponding element content analysis of the titanium alloy samples in SBF lubrication. According to the morphological characterizations (Figure 11a−f,a1−f1), it can be observed that the width of the wear scar on the surface of the Ti64 sample was the largest (∼436 μm), with severe scratches and deep plows and more wear debris. This indicated that the abrasive wear on the surface of the blank titanium alloy sample was serious, while the wear widths of other grooved titanium alloys were relatively narrow, implying that the surface microgroove structure has a positive effect on improving the wear resistance of titanium alloys. This is similar to that in dry friction. Additionally, the element compositions on the worn surface of the titanium alloy samples were detected and analyzed, as seen in Figure 11a2−f2. Si and N elements were found on the surface of the six groups of titanium alloy samples, illustrating the adhesion wear mechanism in the SBF friction process. The surface Si content on the samples were sorted as follows: Ti64 (1.78 wt %) > Ti64-25 (1.35 wt %) > Ti64-35 (1.22 wt %) > Ti64-45 (0.84 wt %), and the Si content

https://doi.org/10.1021/acsomega.2c03166
ACS Omega 2022, 7, 31081−31097

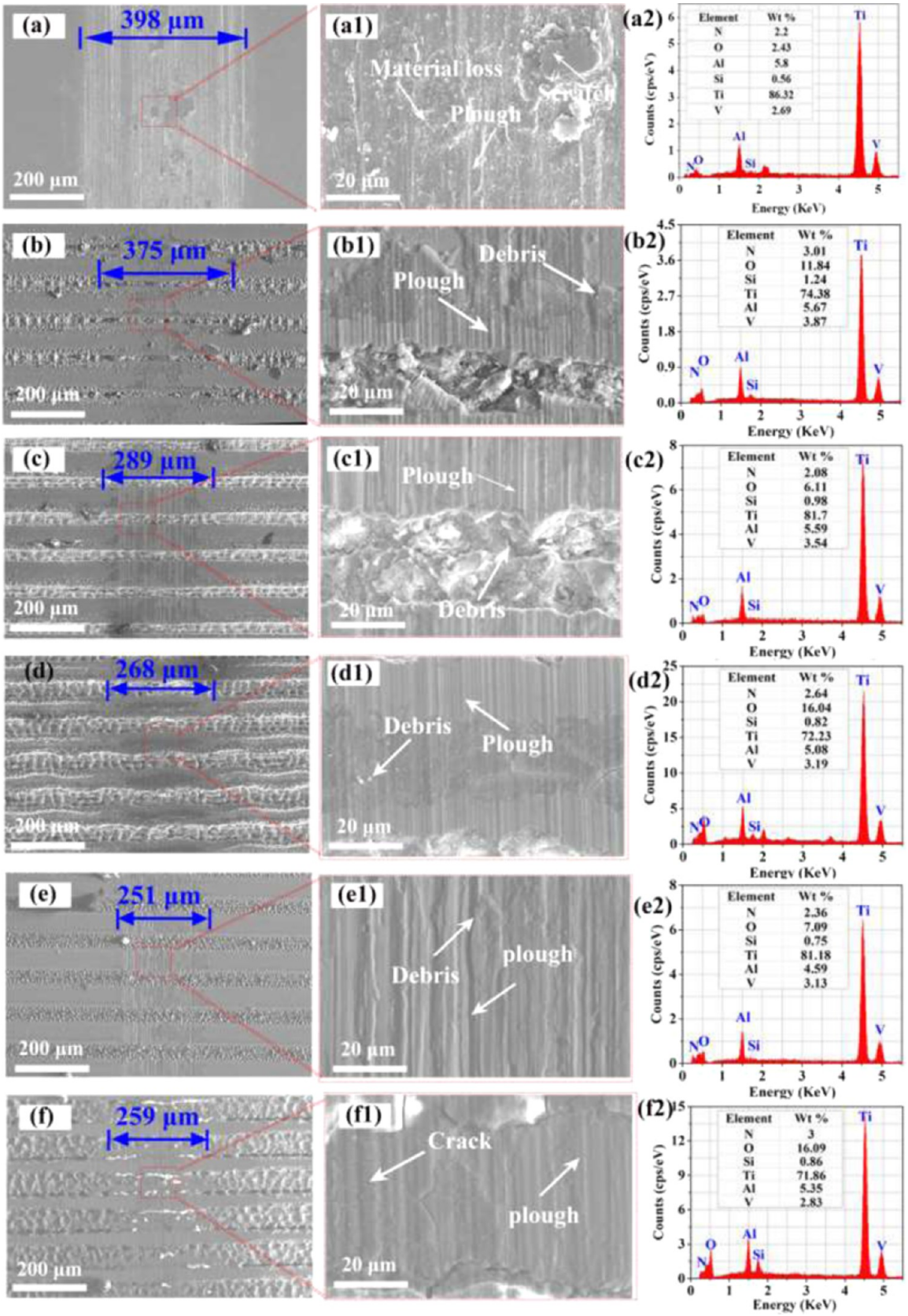

Figure 10. SEM micrographs (a–f and a1–f1) and EDX composition analysis (a2–f2) of worn scars on the Ti–6Al–4V plates before and after texturing under dry friction conditions. (a–a2) Ti64; (b–b2) Ti64-25; (c–c2) Ti64-35; (d–d2) Ti64-45; (e–e2) Ti64-65; and (f–f2) Ti64-65.

of Ti64-55 and Ti64-65 was approximative. The results showed that the adhesion wear resistance of the Ti64 surface was significantly improved through the microgroove structure under SBF lubrication, especially the width of 45 μm. Besides, the

https://doi.org/10.1021/acsomega.2c03166
ACS Omega 2022, 7, 31081–31097

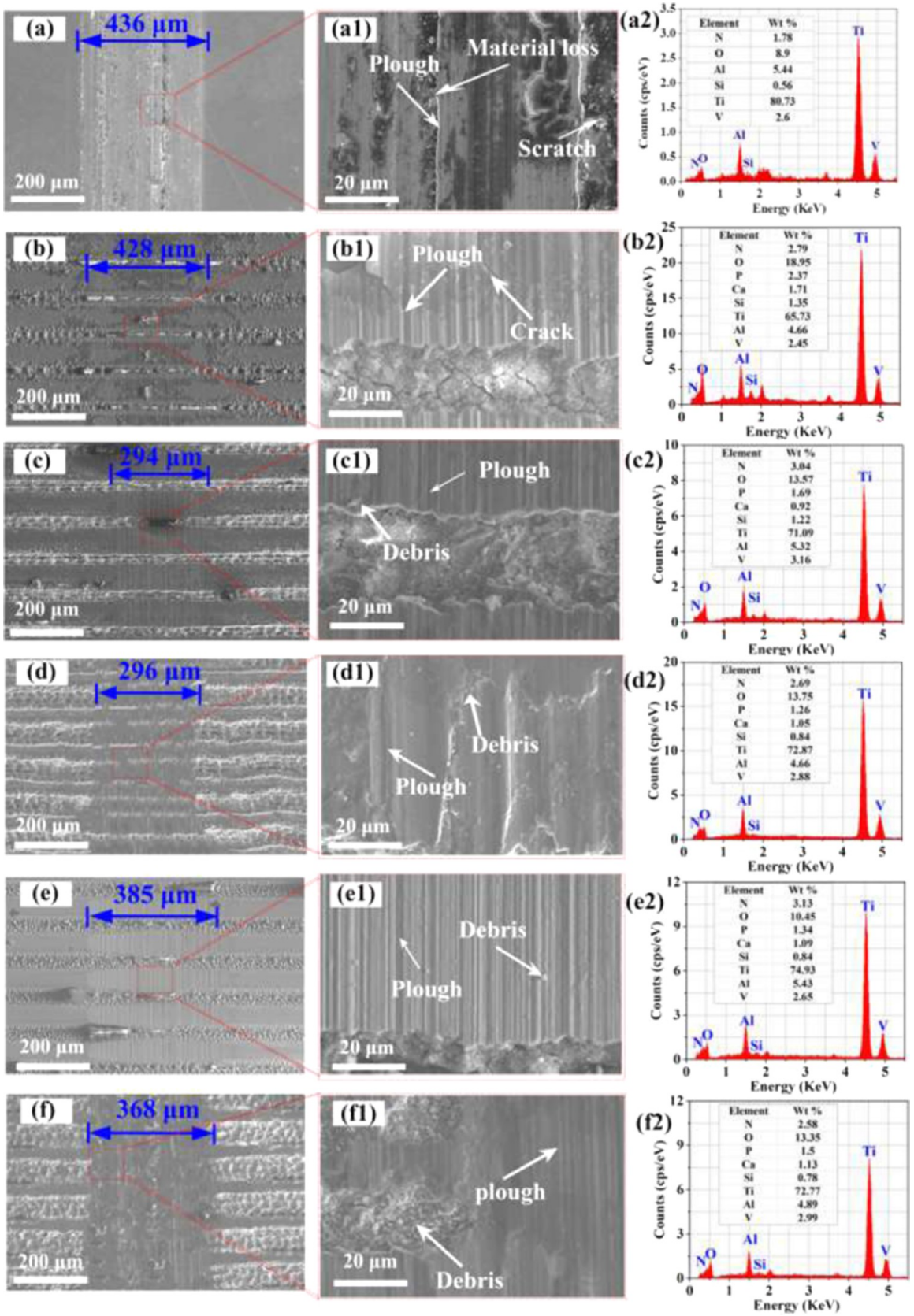

Figure 11. SEM micrographs (a–f and a1–f1) and EDX composition analysis (a2–f2) of worn scars on the Ti–6Al–4V plates before and after texturing under SBF lubrication conditions. (a–a2) Ti64; (b–b2) Ti64-25; (c–c2) Ti64-35; (d–d2) Ti64-45; (e–e2) Ti64-65; and (f–f2) Ti64-65.

occurrence of Ca and P elements on the worn surface of the grooved titanium alloy may be due to the formation of calcium phosphate, induced by the grooved structure in SBF solution. In addition, compared with the wear surface of these samples under

https://doi.org/10.1021/acsomega.2c03166
ACS Omega 2022, 7, 31081–31097

dry friction, wider wear traces were observed in the wet friction process. This also further confirmed the trend of wear rates under both lubrications (Figure 8d). The above analysis results indicated that the abrasive wear and adhesion wear appeared during both lubrication conditions, and the microgroove structure especially with the 45 μm width might have a positive effect on enhancing the wear behavior.

3.9. Biological Activity Evaluation. To study the effect of laser treatment on the biological activity of the titanium alloy surface, the BMSC proliferation and adhesive behavior were analyzed by applying the CCK-8 detection method and a fluorescence microscope. The cell viability results are shown in Figure 12. It can be found that the absorbance of the cells on the

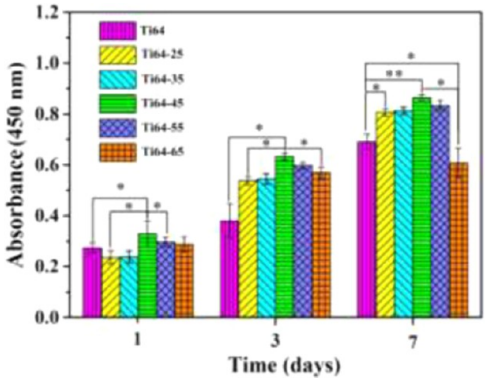

Figure 12. Cell viability of BMSCs by the CCK-8 assay after 1, 3, and 7 days of culture on six different specimens.

six group titanium alloy specimens has increased with increasing culture time, indicating that these titanium alloy materials showed ideal biocompatibility before and after laser treatment. The calculated cell proliferation rates of these six group samples are listed in Table 8, based on the absorbance. It is significant

Table 8. Increasing Cell Proliferation Rates of Samples

	increasing cell proliferation rate (%)		
samples	after 1 day	after 3 days	after 7 days
Ti64	27.8	38.6	68.9
Ti64-25	22.1	51.6	79.6
Ti64-35	22.3	52.0	80.0
Ti64-45	31.7	62.0	84.3
Ti64-55	29.8	59.9	82.5
Ti64-65	28.9	58.4	60.0

that after 1 day of incubation, the surface cell activity of titanium alloy samples with a groove width greater than 45 μm was better than that of Ti64 samples. After culturing for 3 and 7 days, compared with the Ti64 group, the surface of the titanium alloy sample with the groove structure showed a higher cell survival rate, suggesting that the microgroove could improve the BMSC proliferation of the titanium alloy surface. Moreover, the Ti64-45 sample showed the highest cell viability with a cell proliferation rate of 84.3%, indicating that the groove structure with a 45 μm width was more conducive to the BMSC proliferation on the surface.

The adhesion performance of BMSCs on the surface of different titanium alloy samples was observed and shown in Figure 13. Among them, the nucleus and cytoskeleton of BMSCs were, respectively, marked in blue and red colors. It can be

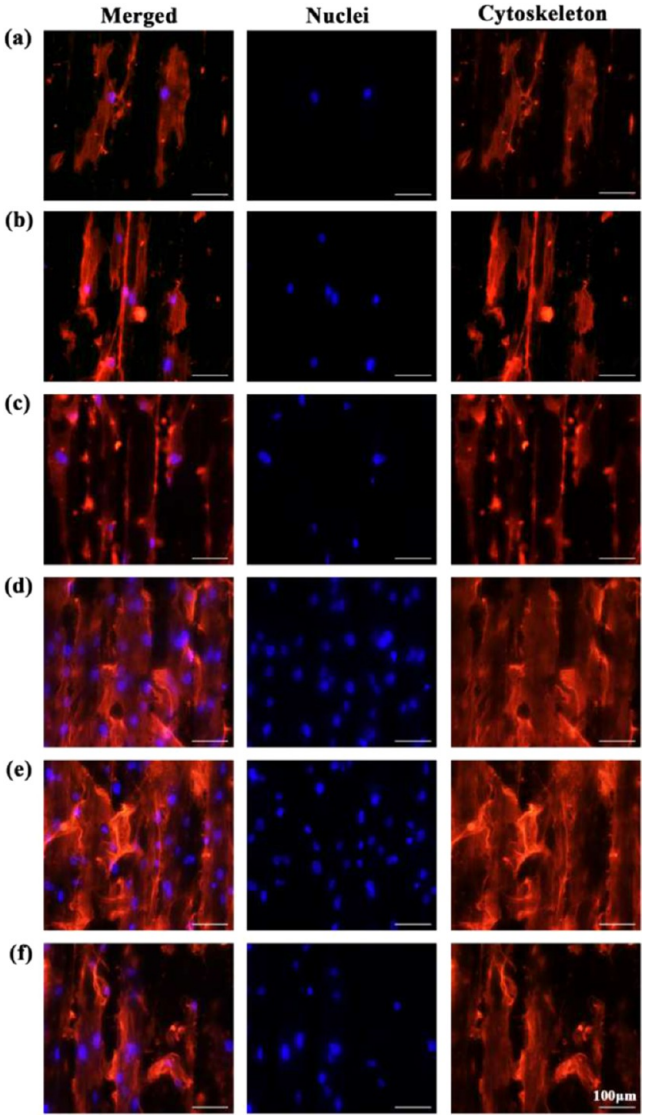

Figure 13. Fluorescence images of BMSCs cultured on six different specimens for 1 day, including blue nucleus images, red cytoskeleton images, and merged fluorescence images. (a) Ti64; (b) Ti64-25; (c) Ti64-35; (d) Ti64-45; (e) Ti64-55; and (f) Ti64-65.

clearly seen that the fluorescent area of the grooved titanium alloy surface was more than that of the Ti64 group, indicating that the BMSCs were prone to adhere to the grooved surface. Moreover, the cells on the surface of Ti64-45 samples were denser than those on the surface of other samples, with a large number of filopodia, further indicating that the groove width of 45 μm was beneficial to the BMSC adhesion. The above bioactivity results demonstrated that the laser treatment with the microgroove structure improved the BMSC adhesion behavior and cell proliferation on the titanium alloy surface, and the optimal groove width was ~45 μm.

4. DISCUSSION

4.1. Electrochemical Corrosion Resistance Mechanism. According to our previous reports,[40] the blank Ti6Al4V alloy might readily corrode in SBF solution, due to the following chemical reactions (Schemes 6–8). During the immersion process of the titanium alloy in the SBF aqueous solution, the hydroxylated titanium compound was first formed and then

https://doi.org/10.1021/acsomega.2c03166
ACS Omega 2022, 7, 31081−31097

reacted with Cl^- and SO_4^{2-} in the SBF solution, further resulting in the corrosion of the titanium alloy surface.

$$Ti - OH_2^+ \leftrightarrow Ti - OH + H^+ \quad (6)$$

$$Ti - OH + Cl^- \rightarrow Ti - Cl + OH^- \quad (7)$$

$$2Ti - OH + SO_4^{2-} \rightarrow Ti_2 - SO_4 + 2OH^- \quad (8)$$

In this study, the corrosion resistance results (Figure 7 and Table 5) showed that the laser microgroove treatment effectively improved the corrosion resistance of the titanium alloy samples in the SBF solution. This result is similar to previous studies.[41] According to this report, laser processing can affect the corrosion rate of the titanium alloy matrix, mainly for the reason that the laser texturing treatment changes the crystal component on the titanium alloy surface.[42] By XRD analysis (Figure 4) and calculated results (Table 4) of the crystal ratio (φ%) of the titanium alloy surface before and after laser treatment, it was found that the φ% value of the grooved titanium alloy surface was reduced compared to the Ti64 sample, indicating that the β phase of the titanium alloy surface has transformed to the α phase during laser ablation. This further implied that the formed remelting layer due to the laser thermal effect might have a refined and uniform tissue structure. As described in the research, the grain refinement on the material surface has a positive effect on reducing the surface defects, thus enhancing its corrosion resistance.[43] In addition, as these reports described,[26,37,44] the galvanic corrosion behavior is the main corrosion form on the surface of the Ti6Al4V alloy, and the density of grain boundaries and grain refinement are the important factors affecting the galvanic corrosion behavior.[44] In this work, according to the microstructure analysis (XRD analysis), it can be obtained that the density of grain boundaries was increased and the microstructures of laser-microgrooved Ti6Al4V samples were refined due to the phase transformation after laser treatment.[37] In the simulated body fluid, the grain refinement improved the passive film formation, which prevented ions from entering the interior of Ti6Al4V, thereby reducing the galvanic corrosion.[26] Therefore, a laser-grooved structure exhibited the improvement of anticorrosion properties on the titanium alloy surface. Compared with the grooved samples of different widths, the Ti64-45 sample has the lowest crystal ratio on the surface, suggesting a more uniform tissue microstructure, thus exhibiting excellent corrosion resistance.

4.2. Wear Resistance Mechanisms. The tribological properties of laser-microgrooved titanium alloys were studied. The experimental results showed that the introduction of the microgroove structure can significantly reduce the friction coefficient between the titanium alloy and Si_3N_4 in dry friction. Moreover, the wear resistance of the titanium alloy surface under dry and SBF lubrications was significantly improved by the laser-grooved structure.

According to Coulomb's law, the friction coefficient (μ) can be calculated by formula 9.[9] In the friction process, the friction coefficient changes with the friction force (F_f), after fixing the normal load (F_n). Johnson et al. mentioned that friction force was mainly related to the adhesion force ($F_{f,adh}$) and surface furrowing effect ($F_{f,pl}$), as shown in formula 10.[45] In these formulas, $F_{f,adh}$ can be determined by formula 11 (τ is the shear strength and A_r is the actual contact area).

$$\mu = \frac{F_f}{F_n} \quad (9)$$

$$F_f = F_{f,adh} + F_{f,pl} \quad (10)$$

$$F_{f,adh} = \tau A_r \quad (11)$$

In the dry friction process, the friction coefficients of the titanium alloy sample with groove structures were lower than those of the blank sample. Based on the surface analysis results (Figure 10), the groove structure might store the wear debris generated during the friction process, resulting in the reduction of wear debris on the surface of the grooved titanium alloy compared to the blank samples. Furthermore, the higher microhardness on the grooved surface would also reduce the shedding of debris, owing to the reduction of residual stress at the interface of the titanium alloy and Si_3N_4 ball during the friction process.[46,47] This might lead to a decrease in deformation friction force. Additionally, after the titanium alloy was treated with laser-microgrooved texturing, the actual contact area at the friction interface became smaller than that on the Ti64 surface, and the shear strength was decreased due to the increase of microhardness. This implied the reduction of adhesive friction force. Hence, the microgrooved titanium alloys showed a lower COF value than the blank Ti64 plate. In addition, compared with the microgrooved samples, the Ti64-45 sample has the largest microhardness (599 HV), indicating a remarkably reduced deformation force. Furthermore, almost no debris was found on the surface of Ti64-45 samples, suggesting the adequacy of entrapment of wear debris with the groove of 45 μm, further reducing the adhesion force. Therefore, Ti64-45 exhibited a smaller friction coefficient (0.215) than other samples in dry sliding. Under SBF lubrication conditions, the microgroove structures can not only be used to store wear debris but also as a lubricant storage tank. However, the existence of the groove structure during the contact process may affect the supply of the lubricant at the contact interface, resulting in the inability to form a sufficiently thick liquid film on the surface. Therefore, under the conditions of SBF lubrication, the friction coefficients on the grooved titanium alloys were higher than that of the blank plate.

In this work, the wear rates and the corresponding ratio of the reducing wear rate after the surface groove texture of the titanium alloy were calculated. It can be found that the laser-grooved treatment can significantly reduce the wear rate on the titanium alloy surface with a reduction of 89.79% under dry friction and 85.43% in SBF lubrication. First, the increase of surface microhardness on the titanium alloys after laser treatment may be an important reason for the improvement of the wear resistance of titanium alloys. This is similar to the report by Kumari et al.[19] The increase of surface hardness would reduce the generation of wear debris on the friction interface, thereby reducing abrasive wear in the friction process. Moreover, according to the analysis results of the chemical composition on the worn surface, the reduction of the Si element on the surface of the grooved titanium alloy also implies that the groove structure can reduce the adhesive wear during the friction process.[48] Therefore, the microgroove structure improved the antiwear properties of the titanium alloy surface significantly. The highest microhardness (599 HV) and the smaller Si (0.98) contents appeared on the Ti64-45 samples, and thus it exhibited superior wear resistance.

4.3. Bioactivity Mechanism Analysis. The excellent bioactivity on the microgrooved titanium alloys was evaluated, by analyzing the BMSC adhesion behavior and proliferation. The results can be explained from the following aspects. First,

https://doi.org/10.1021/acsomega.2c03166
ACS Omega 2022, 7, 31081−31097

compared with the Ti64 group, the surface roughness of the titanium alloy sample with the microgroove structure is significantly increased (Table 3), resulting in the increase of the contact area of BMSCs on the surface, thereby improving the adhesion of the cells.[49,50] Secondly, the surface microgroove structure may affect the contact guidance of cells in the diffusion process.[51,52] As the cells are in contact with the surface, the actin from BMSCs tends to reach an equilibrium state for promoting its self-differentiation on the surface. Due to the influence of the groove structure, the actin filamentous pseudopodia of BMSCs would extend along the direction of the groove, thereby increasing the contact and communication of the cells.[53] This may be an important factor in improving surface cell proliferation. Furthermore, the induced bonelike apatite was found on the microgrooved surface (seen in Figure 13), enhancing the surface bioactivity of the titanium alloy.

In addition, the influence of the groove width on cell behavior might be ascribed to the following two aspects: the BMSCs' extensions and the improved wettability on the groove surface.[54] First, according to our previous reports,[9] the size of BMSCs is ∼50 μm. When the groove width is less than 50 μm, the BMSCs' extensions might appear along the direction of the grooves on the surface, thus promoting cell growth by increasing the possibility of intercellular signaling. Besides, the wettability of the titanium alloy surface is also considered to be the key performance for affecting BMSC behavior. Research in the past reported that the hydrophilic surfaces were prone to induce cell adhesion, proliferation, differentiation, and mineralization.[55] As shown in Figure 5, it is observed that the groove width and surface wettability are positively correlated, implying the improvement of cell behavior on the titanium alloy surface with a greater groove width. Therefore, considering the effect of surface wettability and the microgrooved structure on BMSCs' behavior, Ti64-45 exhibited excellent biological activity due to the improved wettability and the function of promoting BMSC extensions.

5. CONCLUSIONS

In this study, microgroove structures with different widths were prepared on the surface of the titanium alloy by laser processing. The surface morphology, roughness, and the surface properties such as microhardness and wettability were characterized. Furthermore, the electrochemical corrosion performance, tribological properties, and biological activity were systematically investigated. The following conclusions are drawn:

(1) The anticorrosion analysis results showed that the laser-grooved structure improved the corrosion resistance on the titanium alloy surface in SBF solution. Moreover, Ti64-45 showed outstanding anticorrosion properties, resulting from the reduction of the tissue defect. The lowest crystal ratio of the β phase to the α phase on the surface might imply its uniform and dense tissue microstructure and thus exhibit better excellent corrosion resistance.

(2) The tribological performance results showed that the introduction of the microgroove structure can significantly reduce the friction coefficient of the titanium alloy in dry friction. Besides, the wear resistance under both lubrications on the titanium alloy surface was significantly improved. Among them, the wear rates of titanium alloys were reduced by 87% under dry friction and 85% in SBF lubrication, after texturing the microgroove structure with a 45 μm width. This might be mainly related to the increase of the microhardness due to the laser-grooved treatment and the function of storing abrasive particles of the grooved structure.

(3) The in vitro bioactivity results showed that the surface of the titanium alloy samples with microgroove structures exhibited higher BMSC proliferation and adhesion. Moreover, the Ti64-45 sample showed the highest cell viability with a cell proliferation rate of 84.3% and cell adhesion number, which might be ascribed to the improved wettability and the function of promoting BMSC extensions.

The above results imply that the microgroove structure with 45 μm has effectively improved the anticorrosion, antiwear performances, and bioactivity in vitro of the titanium alloy surface. This textured microgroove structure has potential application prospects in the field of titanium alloy orthopedic implants.

■ ASSOCIATED CONTENT

Supporting Information

The Supporting Information is available free of charge at https://pubs.acs.org/doi/10.1021/acsomega.2c03166.

Table of Ti6Al4V alloy compositions and the table of SBF solution compositions (PDF)

■ AUTHOR INFORMATION

Corresponding Authors

Chenchen Wang − *School of Chemical and Environmental Engineering, Shanghai Institute of Technology, 201418 Shanghai, China; School of Chemistry and Chemical Engineering, Shanghai Jiao Tong University, 200240 Shanghai, China;* orcid.org/0000-0003-0193-3593; Email: wangchenchen76@163.com

Sheng Han − *School of Chemical and Environmental Engineering, Shanghai Institute of Technology, 201418 Shanghai, China; School of Chemistry and Chemical Engineering, Shihezi University, 832003 Shihezi, China;* orcid.org/0000-0001-9631-2743; Email: hansheng654321@sina.com

Xin Zhao − *Shanghai Key Laboratory of Orthopaedic Implants, Department of Orthopaedic Surgery, Shanghai Ninth People's Hospital, Shanghai Jiao Tong University School of Medicine, 200041 Shanghai, China*; Email: zhaoxinmlg@126.com

Authors

Panpan Tian − *School of Chemistry and Chemical Engineering, Shihezi University, 832003 Shihezi, China*

Hao Cao − *School of Chemical and Environmental Engineering, Shanghai Institute of Technology, 201418 Shanghai, China*

Bin Sun − *School of Chemical and Environmental Engineering, Shanghai Institute of Technology, 201418 Shanghai, China*

Jincan Yan − *School of Chemical and Environmental Engineering, Shanghai Institute of Technology, 201418 Shanghai, China*

Yuan Xue − *School of Chemical and Environmental Engineering, Shanghai Institute of Technology, 201418 Shanghai, China*

Hualin Lin − *School of Chemical and Environmental Engineering, Shanghai Institute of Technology, 201418 Shanghai, China*

https://doi.org/10.1021/acsomega.2c03166
ACS Omega 2022, 7, 31081−31097

Tianhui Ren − *School of Chemistry and Chemical Engineering, Shanghai Jiao Tong University, 200240 Shanghai, China;* orcid.org/0000-0003-4369-9678

Complete contact information is available at: https://pubs.acs.org/10.1021/acsomega.2c03166

Author Contributions

⊥C.W. and P.T. contributed equally to this work.

Notes

The authors declare no competing financial interest.

■ ACKNOWLEDGMENTS

The authors are grateful to the Shanghai "Science and Technology Innovation Action Plan" Morning Star Cultivation (Sailing Program 22YF1447500), and Innovation Fund (Grant No. IFPM2019A006) of the Joint Research Center for Precision Medicine established by the Shanghai Jiao Tong University & Affiliated Sixth People's Hospital South Campus (Fengxian Central Hospital), and the Shanghai Jiao Tong University "Jiao Tong University Star" Project Medical-Industrial Cross-Research Fund (Grant No. YG2021QN98).

■ ABBREVIATIONS

BMSCs, bone marrow mesenchymal stem cells; APTES, 3-aminopropyltriethoxysilane; DA, dopamine; Ti64, untreated Ti6Al4V; Ti64-25, microgrooved Ti6Al4V with a width of 25 μm; Ti64-35, microgrooved Ti6Al4V with a width of 35 μm; Ti64-45, microgrooved Ti6Al4V with a width of 45 μm; Ti64-55, microgrooved Ti6Al4V with a width of 55 μm; Ti64-65, microgrooved Ti6Al4V with a width of 65 μm; CCK-8, cell counting kit-8; ATR-FTIR, attenuated total reflection from Fourier transform infrared; SEM, scanning electron microscopy; EDX, energy-dispersive X-ray; XPS, X-ray photoelectron spectroscopy; CA, contact angle; VCA, vertical observation of the contact angle; PCA, parallel observation of the contact angle; SBF, simulated body fluid; α-MEM, MEM alpha modification; COF, friction coefficients; ACOF, average coefficient of friction

■ REFERENCES

(1) Wei, X.; Zhang, Y.; Feng, H.; Cao, X.; Ding, Q.; Lu, Z.; Zhang, G. Bio-Tribology and Corrosion Behaviors of a Si- and N-Incorporated Diamond-like Carbon Film: A New Class of Protective Film for Ti6Al4V Artificial Implants. *ACS Biomater. Sci. Eng.* **2022**, *8*, 1166−1180.

(2) Choy, M. T.; Tang, C. Y.; Chen, L.; Wong, C. T.; Tsui, C. P. In vitro and in vivo performance of bioactive Ti6Al4V/TiC/HA implants fabricated by a rapid microwave sintering technique. *Mater. Sci. Eng. C* **2014**, *42*, 746−756.

(3) Zheng, B.; Dong, F.; Yuan, X.; Huang, H.; Zhang, Y.; Zuo, X.; Luo, L.; Wang, L.; Su, Y.; Li, W.; Liaw, P. K.; Wang, X. Microstructure and tribological behavior of in situ synthesized (TiB+TiC)/Ti6Al4V (TiB/TiC=1/1) composites. *Tribol. Int.* **2020**, *145*, No. 106177.

(4) Wang, C.; Zhang, G.; Li, Z.; Zeng, X.; Xu, Y.; Zhao, S.; Hu, H.; Zhang, Y.; Ren, T. Tribological behavior of Ti-6Al-4V against cortical bone in different biolubricants. *J. Mech. Behav. Biomed. Mater.* **2019**, *90*, 460−471.

(5) Zhao, Z.; Zhang, L.; Bai, P.; Du, W.; Wang, S.; Xu, X.; Dong, Q.; Li, Y.; Han, B. Tribological Behavior of In Situ TiC/Graphene/Graphite/Ti6Al4V Matrix Composite Through Laser Cladding. *Acta Metall. Sin.* **2021**, *34*, 1317−1330.

(6) Tillmann, W.; Lopes Dias, N. F.; Franke, C.; Kokalj, D.; Stangier, D.; Filor, V.; Mateus-Vargas, R. H.; et al. Tribo-mechanical properties and biocompatibility of Ag-containing amorphous carbon films deposited onto Ti6Al4V. *Surf. Coat. Technol.* **2021**, *421*, No. 127384.

(7) Wang, C.; Hu, H.; Li, Z.; Shen, Y.; Xu, Y.; Zhang, G.; Zeng, X.; Deng, J.; Zhao, S.; Ren, T.; Zhang, Y. Enhanced Osseointegration of Titanium Alloy Implants with Laser Microgrooved Surfaces and Graphene Oxide Coating. *ACS Appl. Mater. Interfaces* **2019**, *11*, 39470−39483.

(8) Wang, C.; Li, Z.; Zhao, H.; Zhang, G.; Ren, T.; Zhang, Y. Enhanced anticorrosion and antiwear properties of Ti−6Al−4V alloys with laser texture and graphene oxide coatings. *Tribol. Int.* **2020**, *152*, No. 106475.

(9) Wang, C.; Zhang, G.; Li, Z.; Xu, Y.; Zeng, X.; Zhao, S.; Deng, J.; Hu, H.; Zhang, Y.; Ren, T. Microtribological properties of Ti 6Al 4V alloy treated with self-assembled dopamine and graphene oxide coatings. *Tribol. Int.* **2019**, *137*, 46−58.

(10) Pfleging, W.; Kumari, R.; Besser, H.; Scharnweber, T.; Majumdar, J. D. Laser surface textured titanium alloy (Ti−6Al−4V): Part 1 − Surface characterization. *Appl. Surf. Sci.* **2015**, *355*, 104−111.

(11) Kaliaraj, G. S.; Sivab, T.; Ramadoss, A. Surface functionalized bioceramics coated on metallic implants for biomedical and anticorrosion performance − a review. *J. Mater. Chem. B* **2021**, *9*, 9433−9460.

(12) Liu, Y.; Su, J.; Tan, C.; Feng, Z.; Zhang, H.; Wu, L.; Chen, B.; Song, X. Effect of laser texturing on mechanical strength and microstructural properties of hot-pressing joining of carbon fiber reinforced plastic to Ti6Al4V. *J. Manuf. Processes* **2021**, *65*, 30−41.

(13) Ju, J.; Zhao, C.; Kang, M.; Li, J.; He, L.; Wang, C.; Li, J.; Fu, H.; Wang, J. Effect of heat treatment on microstructure and tribological behavior of Ti−6Al−4V alloys fabricated by selective laser melting. *Tribol. Int.* **2021**, *159*, No. 106996.

(14) Ding, J.; Zou, S.; Choi, J.; Cui, J.; Yuan, D.; Sun, H.; Wu, C.; Zhu, J.; Ye, X.; Su, X. A laser texturing study on multi-crystalline silicon solar cells. *Sol. Energy Mater. Sol. Cells* **2020**, *214*, No. 110587.

(15) Chen, J.; Li, J.; Hu, F.; Zou, Q.; Mei, Q.; Li, S.; Hao, Y.; Hou, W.; Li, J.; Li, Y.; Zuo, Y. Effect of Microarc Oxidation-Treated Ti6Al4V Scaffold Following Low-Intensity Pulsed Ultrasound Stimulation on Osteogenic Cells in Vitro. *ACS Biomater. Sci. Eng.* **2019**, *5*, 572−581.

(16) Wu, Z.; Xing, Y.; Huang, P.; Liu, L. Tribological properties of dimple-textured titanium alloys under dry sliding contact. *Surf. Coat. Technol.* **2017**, *309*, 21−28.

(17) Lu, X.; Khonsari, M. M. An Experimental Investigation of Dimple Effect on the Stribeck Curve of Journal Bearings. *Tribol. Lett.* **2007**, *27*, 169−176.

(18) Xu, Y.; Li, Z.; Zhang, G.; Wang, G.; Zeng, Z.; Wang, C.; Wang, C.; Zhao, S.; Zhao, S.; Zhang, Y.; Zhang, Y.; Ren, T. Electrochemical corrosion and anisotropic tribological properties of bioinspired hierarchical morphologies on Ti-6Al-4V fabricated by laser texturing. *Tribol. Int.* **2019**, *134*, 352−364.

(19) Kumari, R.; Scharnweber, T.; Pfleging, W.; Besser, H.; Majumdar, J. D. Laser surface textured titanium alloy (Ti−6Al−4V) − Part II − Studies on bio-compatibility. *Appl. Surf. Sci.* **2015**, *357*, 750−758.

(20) Chong, P. H.; Liu, Z.; Skeldon, P.; Crouse, P. Characterisation and corrosion performance of laser-melted 3CR12 steel. *Appl. Surf. Sci.* **2005**, *247*, 362−368.

(21) Conradi, M.; Kocijan, A.; Klobčar, D.; Podgornik, B. Tribological response of laser-textured Ti6Al4V alloy under dry conditions and lubricated with Hank's solution. *Tribol. Int.* **2021**, *160*, No. 107049.

(22) Xu, X.; Lu, Y.; Li, S.; Guo, S.; He, M.; Luo, K.; Lin, J. Copper-modified Ti6Al4V alloy fabricated by selective laser melting with pro-angiogenic and anti-inflammatory properties for potential guided bone regeneration applications. *Mater. Sci. Eng. C* **2018**, *90*, 198−210.

(23) Wang, Y.; Yu, Z.; Li, K.; Hu, J. Study on the effect of surface characteristics of short-pulse laser patterned titanium alloy on cell proliferation and osteogenic differentiation. *Mater. Sci. Eng. C* **2021**, *128*, No. 112349.

(24) Jain, A.; Bajpai, V. Mechanical micro-texturing and characterization on Ti6Al4V for the improvement of surface properties. *Surf. Coat. Technol.* **2019**, *380*, No. 125087.

(25) Cao, L.; Chen, Y.; Cui, J.; Li, W.; Lin, Z.; Zhang, P. Corrosion Wear Performance of Pure Titanium Laser Texturing Surface by Nitrogen Ion Implantation. *Metals* **2020**, *10*, 990−1000.
(26) Conradi, M.; Kocijan, A.; Klobčar, D.; Godec, M. Influence of Laser Texturing on Microstructure, Surface and Corrosion Properties of Ti-6Al-4V. *Metals* **2020**, *10*, 1504−1513.
(27) Yu, Z.; Yin, S.; Zhang, W.; Jiang, X.; Hu, J. Picosecond laser texturing on titanium alloy for biomedical implants in cell proliferation and vascularization. *J. Biomed. Mater. Res. B* **2020**, *108*, 1494−1504.
(28) Tian, P.; Zhao, X.; Sun, B.; Cao, H.; Zhao, Y.; Yan, J.; Xue, Y.; Lin, H.; Han, S.; Ren, T.; Wang, C. Enhanced anticorrosion and tribological properties of Ti6Al4V alloys with Fe_3O_4/HA coatings. *Surf. Coat. Technol.* **2022**, *433*, No. 128118.
(29) Bhaduri, D.; Batal, A.; Dimov, S. S.; Zhang, Z.; Dong, H.; Fallqvist, M.; M'Saoubi, R. On Design and Tribological Behaviour of Laser Textured Surfaces. *Procedia CIRP* **2017**, *60*, 20−25.
(30) Raimbault, O.; Benayoun, S.; Anselme, K.; Mauclair, C.; Bourgade, T.; Kietzig, A.; Girard-Lauriault, P.; Valette, S.; Donnet, C. The effects of femtosecond laser-textured Ti-6Al-4V on wettability and cell response. *J. Mater. Sci. Eng. C* **2016**, *69*, 311−320.
(31) Gui, N.; Xu, W.; Abraham, A.; Shukla, R.; Qian, M. Osteoblast Responses to Titanium-Coated Subcellular Scaled Microgrooves. *ACS Appl. Bio Mater.* **2019**, *2*, 2405−2413.
(32) Cui, C. Y.; Hong, Y. J.; Ye, J. F.; Wen, M.; Li, N. L. Effects of laser energy density on impulse coupling coefficient of laser ablation of water for propulsion. *Appl. Phys. A* **2011**, *103*, 239−243.
(33) Ehtemam-Haghighi, S.; Liu, Y.; Cao, G.; Zhang, L. C. Influence of Nb on the $\beta \rightarrow \alpha''$ martensitic phase transformation and properties of the newly designed Ti-Fe-Nb alloys. *Mater. Sci. Eng. C* **2016**, *60*, 503−510.
(34) Çelen, S.; Özden, H. Laser-induced novel patterns, As smart strain actuators for new-age dental implant surfaces. *Appl. Surf. Sci.* **2012**, *263*, 579−585.
(35) Vora, H. D.; Santhanakrishnan, S.; Harimkar, S. P.; Boetcher, S. K. S.; Dahotre, N. B. One-dimensional multipulse laser machining of structural alumina, evolution of surface topography. *Int. J. Adv. Des. Manuf. Technol.* **2013**, *68*, 69−83.
(36) Zhang, Q.; Chen, J.; Guo, P.; Tan, H.; Lin, X.; Huang, W. Texture and microstructure characterization in laser additive manufactured Ti−6Al−2Zr−2Sn−3Mo−1.5Cr−2Nb titanium alloy. *Mater. Des.* **2015**, *88*, 550−557.
(37) Zafari, A.; Barati, M. R.; Xia, K. Controlling martensitic decomposition during selective laser melting to achieve best ductility in high strength Ti-6Al-4V. *Mater. Sci. Eng. A* **2019**, *744*, 445−455.
(38) Ju, J.; Li, J.; Jiang, M.; Li, M.; Yang, L. X.; Wang, K.; Yang, C.; Kang, M.; Wang, J. Microstructure and electrochemical corrosion behavior of selective laser melted Ti−6Al−4V alloy in simulated artificial saliva. *Trans. Nonferrous Met. Soc.* **2021**, *31*, 167−177.
(39) Ma, C.; Bai, S.; Peng, X.; Meng, Y. Anisotropic wettability of laser micro-grooved SiC surfaces. *Appl. Surf. Sci.* **2013**, *284*, 930−935.
(40) Karimi, S.; Alfantazi, A. Electrochemical Corrosion Behavior of Orthopedic Biomaterials in Presence of Human Serum Albumin. *J. Electrochem. Soc.* **2013**, *160*, C206−C214.
(41) Kuczyńska-Zemła, D.; Sotniczuk, A.; Pisarek, M.; Chlanda, A.; Garbacz, H. Corrosion behavior of titanium modified by direct laser interference lithography. *Surf. Coat. Technol.* **2021**, *418*, No. 127219.
(42) Zhao, X.; Zhang, H.; Liu, H.; Li, S.; Li, W.; Wang, X. In vitro bio-tribological behaviour of textured nitride coating on selective laser melted Ti-6Al-4V alloy. *Surf. Coat. Technol.* **2021**, *409*, No. 126904.
(43) Amanov, A. Advancement of tribological properties of Ti−6Al−4V alloy fabricated by selective laser melting. *Tribol. Int.* **2021**, *155*, No. 106806.
(44) Fazel, M.; Salimijazi, H. R.; Golozar, M. A.; Garsivaz jazi, M. R. A comparison of corrosion, tribocorrosion and electrochemical impedance properties of pure Ti and Ti6Al4V alloy treated by micro-arc oxidation process. *Appl. Surf. Sci.* **2015**, *324*, 751−756.
(45) Johnson, K. L.; Greenwood, J. A. An Adhesion Map for the Contact of Elastic Spheres. *J. Colloid Interface Sci.* **1997**, *192*, 326−333.
(46) Deng, G.; Zhao, X.; Su, L.; Wei, P.; Zhang, L.; Zhan, L.; Chong, Y.; Zhu, H.; Tsuji, N. Effect of high pressure torsion process on the microhardness, microstructure and tribological property of Ti6Al4V alloy. *J. Mater. Sci. Technol.* **2021**, *94*, 183−195.
(47) Singh, A. K.; Narasimhan, K.; Singh, R. Finite element analysis of thermomechanical behavior and residual stresses in cold flowformed Ti6Al4V alloy. *Int. J. Adv. Des. Manuf. Technol.* **2019**, *103*, 1257−1277.
(48) Chen, F. X.; Mai, Y. J.; Xiao, Q. N.; Cai, G. F.; Zhang, L. Y.; Liu, C. S.; Jie, X. H. Three-dimensional graphene nanosheet films towards high performance solid lubricants. *Appl. Surf. Sci.* **2019**, *467−468*, 30−36.
(49) Deligianni, D. D.; Katsala, N. S.; Ladas, D.; Sotiropoulou, J. Amedee. Effect of surface roughness of the titanium alloy Ti-6Al-4V on human bone marrow cell response and on protein adsorption. *Biomaterials* **2001**, *22*, 1241−1251.
(50) Wan, Y.; Wang, Y.; Liu, Z.; Qu, X.; Han, B.; Bei, J.; Wang, S. Adhesion and proliferation of OCT-1 osteoblast-like cells on micro- and nano-scale topography structured poly(L-lactide). *Biomaterials* **2005**, *26*, 4453−4459.
(51) Mwenifumbo, S.; Herman, P. R.; Li, M.; Fieret, J.; Pique, A.; Soboyejo, W.; Okada, T.; Bachmann, F. G.; Hoving, W.; Washio, K.; Xu, X.; Dubowski, J. J.; Geohegan, D. B.; Traeger, F. Cell/surface interactions on laser-micro-textured titanium-coated silicon surfaces. *Photon Process. Microelectron. Photonics III* **2004**, *5339*, 214−225.
(52) Santoro, F.; van de Burgt, Y.; Keene, S.; Cui, B.; Salleo, A. Enhanced Cell-Chip Coupling by Rapid Femtosecond Laser Patterning of Soft PEDOT,PSS Biointerfaces. *ACS Appl. Mater. Interfaces* **2017**, *9*, 39116−39121.
(53) Bayrak, Ö.; Asl, H. G.; Ak, A. Protein adsorption, cell viability and corrosion properties of Ti6Al4V alloy treated by plasma oxidation and anodic oxidation. *Int. J. Miner. Metall. Mater.* **2020**, *27*, 1269−1280.
(54) Ricci, J. L.; Alexander, H. Laser Microtexturing of Implant Surfaces for Enhanced Tissue Integration. *Key Eng. Mater.* **2001**, *198−199*, 179−202.
(55) Tseng, S.-J.; Cheng, C.; Lee, T.; Lin, J. Studies of osteoblast-like MG-63 cellular proliferation and differentiation with cyclic stretching cell culture system on biomimetic hydrophilic layers modified polydimethylsiloxane substrate. *Biochem. Eng. J.* **2021**, *168*, No. 107946.

https://doi.org/10.1021/acsomega.2c03166
ACS Omega 2022, 7, 31081−31097